Lab on a Chip

Static droplet array for culturing single live adherent cells in an isolated chemical microenvironment

Journal:	*Lab on a Chip*
Manuscript ID	LC-ART-04-2018-000403.R1
Article Type:	Paper
Date Submitted by the Author:	05-Jun-2018
Complete List of Authors:	Hassanzadeh-Barforoushi, Amin; University of New South Wales, Law, Andrew; Garvan Institute of Medical Research Hejri, Abbas ; Macquarie University Faculty of Science and Engineering Asadnia, Mohsen; Macquarie University, Engineering Gallego-Ortega, David ; Garvan Institute of Medical Research Ormandy, Christopher ; Garvan Institute of Medical Research Ebrahimi Warkiani, Majid; University of New South Wales , Mechanical and Manufacturing

Static droplet array for culturing single live adherent cells in an isolated chemical microenvironment

Amin Hassanzadeh-Barforoushi[1,2*], Andrew M. K. Law[2], Abbas Hejri[3], Mohsen Asadnia[3], Christopher J. Orman dy[2, 4], David Gallego-Ortega[2, 4], and Majid Ebrahimi Warkiani[5,6*]

[1]School of Mechanical and Manufacturing Engineering, University of New South Wales, Sydney, NSW 2052, Australia
[2] Cancer Division, Garvan Institute of Medical Research/ the Kinghorn Cancer Centre, Sydney, NSW 2010, Australia
[3]Department of Engineering, Faculty of Science, Macquarie University, Sydney, NSW 2109, Australia
[4]St Vincent's Clinical School, Faculty of Medicine, University of New South Wales, Sydney, NSW 2052, Australia
[5]School of Biomedical Engineering and Institute for Biomedical Materials & Devices (IBMD), University of Technology Sydney, Sydney, NSW 2007, Australia
[6] Institute of Molecular Medicine, Sechenov First Moscow State University, Moscow 119991, Russia

* Contact

Amin Hassanzadeh-Barforoushi (a.hassanzadehbarforoushi@unsw.edu.au)
School of Mechanical and Manufacturing Engineering, University of New South Wales, Sydney, NSW 2052, Australia

Majid Ebrahimi Warkiani (majid.warkiani@uts.edu.au)
School of Biomedical Engineering, University of Technology Sydney, Sydney, NSW 2007, Australia

Abstract

We present here a new method to easily and reliably generate an array of hundreds of dispersed nanoliter-volume semi-droplets for single-cells culture and analysis. The liquid segmentation step occurs directly in indexed traps by a tweezer-like mechanism and is stabilized by spatial confinement. Unlike common droplet-based techniques, the semi-droplet wets its surrounding trap walls thus supporting the culturing of both adherent and non-adherent cells. To eliminate cross-droplet cell migration and chemical cross-talk each semi-droplet is separated from nearby trap by a ~80 pL air plug. The overall setup and injection procedure takes less than 10 minutes, is insensitive to fabrication defects and supports cell recovery for downstream analysis. The method offers a new approach to easily capture, image and culture single cells in a chemically isolated microenvironment as a preliminary step towards high-throughput single-cell assays.

***Keywords*:** Microfluidics; Static droplet array; Single-cell analysis; MMP activity; Cancer heterogeneity

Introduction

Over the past decade, studying cells at the single cell level has attracted growing interest in cancer research[1, 2], stem cell research[3, 4], immunology[5, 6] and neuroscience[7]. Since measuring the collective behaviour of bulk cell populations only provides the average response, each individual cell acts differently depending on its transcriptional state, biological context, and the microenvironment[8-10]. Therefore, single cell analysis allows capturing heterogeneity that exists within the cell population at the cellular and molecular (subcellular) level[8, 11]. This transition to single cell analysis entailed a broad range from unravelling single cell's genome[12] and transcriptome[13] to studying secreted proteins and biomolecules of each single cell[14, 15]. Despite these inclinations, no effective tool has been proposed until the advent of MEMS technology, as manipulation of single cells and positioning cells in spatially separate locations remained too much of a challenge. Microfluidic devices are capable of handling pico-liter to sub-microliter volumes of liquids and therefore are suitable for manipulating volumes comparable to the volume of single cells. These include microwells[16], micropatterns[17], single cell traps[18], and micropillars[19] all of which are capable of spatially confining single cells for further downstream analysis. The development of each of these devices can be tailored to the specific application and data sought[20].

Flow cytometry is the most widely used technique for high-throughput single-cell analysis and is improved with the introduction of CYTOF[21, 22] (Time of Flight Mass Cytometry, Fluidigm, USA) which enables looking at several biomarkers at a time using transition element isotopes. However, it cannot track single-cells over time and therefore has limited capability to associate cell biomarkers with dynamic cell behaviour. Unlike flow cytometry, time-lapse microscopy can track thousands of cells in parallel while correlating their morphology and dynamic gene expression patterns to selected reporter genes[23, 24]. In spite of these advantages, determining the contribution of single-cell secretion and paracrine

signalling to the overall cell response is not possible due to the shared soluble media present in static culture. To accomplish this goal, cells must be kept in separate compartments where their viability and growth can be maintained over extended period of culture. The compartmentalization of individual live cells in pico- to nano-liter volume water-in-oil droplets has complemented these technologies by spatially confining cell-secreted biomolecules to a droplet thus maintaining the single cell chemical signature[25, 26].

In spite of significant progress of droplet-based platforms, the manipulation of single droplets remains challenging. Among these challenges are the ability to control droplet generation on demand, droplet coalescence, re-adjustment of a droplet's volume, and droplet splitting and sorting[27, 28]. Several microfluidic devices have been proposed that use surface properties to manipulate and separate droplets[29] including use of superhydrophobic surfaces[30], surface anisotropy[31], and droplet dispensing on hydrophobic surfaces[32]. However, their use of surface properties and external equipment makes them difficult to operate and may disturb encapsulated cell's function. Non-microfluidic droplet manipulation techniques[33, 34] can eliminate the need for expertise in liquid handling but their throughput is much lower compared to microfluidic approaches; and since droplets are not sheathed, cross-contamination with the outside environment are challenging. Perhaps one of the least addressed manipulation capabilities is droplet immobilization in an indexed array, which is an essential step towards single cell tracking over time scales of hours up to days.

Most of the existing methods for generating stationary droplet arrays rely on the generation of droplets or plugs of dispersed media in a channel primed with oil. In the systems where droplets are made in a continuous oil phase, an array of traps is designed to immobilize the generated droplets[35-38]. Therefore, these methods necessitate delicate production and manipulation of droplets with the volumes of the nanowell/trap size. In addition, the pressure coupling of droplet generation and droplet trapping requires precise adjustment of the loading

pressure and therefore rely on complex tubing and automation[39]. Systems introducing plugs of liquid sample into oil are able to produce and capture droplets at the same time but they either rely on multilayer photolithography[40] or computer-controlled microvalving system[41] as well as peripheral equipment like pumps[42].

Since droplets in most of the previous studies are sheathed with oil on all sides, they can only accommodate suspended cells and are not able to support long term incubation of adherent cells[43-45]. In addition, live cells are prone to anoikis in droplets due to loss of anchorage to a substrate and disruption in cell attachment[46, 47].

A new approach that overcomes these issues with the ability to easily segment the liquid into indexed stationary traps and support live cell culturing was recently presented[48, 49]. Although it successfully outperformed other methods in terms of simplicity, portability and cell recovery it relies on a defect-free fabrication of all traps, which is challenging. We present here a new method to easily generate hundreds of stationary semi-droplets in indexed traps for live cell incubation and tracking. The method does not require microfluidic expertise, uses microliter volume of reagents, can be easily tailored to the desired droplet volume, is operated with standard laboratory pipette and is highly robust.

Materials and Methods

Device design and fabrication

Deep Reactive Ion Etching (DRIE) on silicon on insulator (SOI) wafer was employed to achieve aspect ratios as high as 1:8. Briefly, the device pattern was designed using the AutoCAD 2015 software (Autodesk®) and printed on a glass mask. The mask was then used to make patterns on a SOI wafer (100mm wafer diameter, 80±1 μm device layer, 2 μm buried oxide layer, and 500±15 μm handle layer) coated with nLOF2020 photoresist using a Karl Suss MA6 Mask Aligner (SUSS MicroTec, Germany) followed by DRIE using a STS system.

Cell culture

Breast cancer cell line MDA-MB-231(ATCC® HTB-26™) was cultured under standard conditions of 95% humidity and 5% CO2 in RPMI medium (Gibco, 11875) with 10% FBS, 1% penicillin/streptomycin, and 6% insulin in a T-75 flask and with seeding density of 10^4 cells/cm^2 and passaged at 80% confluency.

Device preparation and set up

The patterned SOI wafer was silanized carefully using vaporized trichloro (1H, 1H, 2H, 2H-perfluorooctyl) silane (Sigma Aldrich, USA) in a vacuum chamber over night to render the surface hydrophobic for easier release of cured PDMS. PDMS (Sylgard 184, Dow Corning, USA) was prepared by mixing elastomer and curing agent in a standard ratio of 10:1 followed by degassing in a vacuum chamber for 1 hour. The mixture was then poured onto SOI mould, and cured at 80 °C for 2 hours before peeling. The PDMS was then cut from the mould and inlet and outlet access holes were made using 1.5 mm biopsy punch. The fabricated devices were brought in conformal contact with the substrate and, if necessary, pressed together to create a seal.

Cell loading and single cell monitoring

Cells were prepared with a range of concentrations to capture single cells. To examine the trap occupancy, different cell concentrations were made and tested. One confluent flask of MDA-MB-231 cancer cells was first trypsinized and cells were suspended in appropriate volume of fresh medium. Cells were then counted using countess (Invitrogen) and cell viability of >90% was ensured. For injection into the microfluidic chips, the cell suspension was mixed well and for each chip 20 µl (for the device with smaller trap size) and 40 µl (for the device with bigger trap size) was used. Devices were maintained in a humidity chamber (Fig. S1) and were monitored after 6 hours for cell attachment.

On-chip live/dead staining experiment

Cells were first cultured in the device using pipette injection and incubated for 24 hours. Live/dead double staining kit (Sigma-Aldrich 04511, St. Louis, MO, USA) containing calcein AM and propidium iodide (PI) solutions staining live and dead cells respectively were used. A 4 μM staining solution was injected into the device and cells were incubated for 1 hr followed by on-chip PBS wash.

Cell viability and proliferation assay

To assess cell viability in the chip, cell concentration which gives the highest number of single cell traps were used for device loading (Fig. 3). Five devices were used for viability measurement at each time points of 12 hrs, 18 hrs, 24 hrs, and 48 hrs (12 experiments in total). At each time point, first a device was removed from the humidity chamber and Trypan blue (Thermofisher, Waltham, MA, USA) was injected into the device. The device was immediately imaged under the microscope. In order to measure proliferation, devices were imaged at three time points of 6 hrs, 24 hrs and 48 hrs.

Matrix metalloproteinase (MMP) assay

Fluorescence resonance energy transfer (FRET)-based polypeptide MMP substrate PEPDAB008 (Biozyme, Apex, NC, USA) was diluted to 40 μM in 50mM Tris buffer (150mM NaCl, 2mM $CaCl_2$, 5 μM $ZnSO_4$, and 0.01% Brij-35; PH 7.5). Cell concentration of 7×10^5/ml was prepared and 2.5nl device was used in all experiments. Before injection into the device, cell suspension and MMP substrate were mixed in 1:1 volume ratio. Therefore, the final cell and substrate concentration were 3.5×10^5/ml and 20 μM respectively. Immediately after injection, shearing and sheathing with oil, the device was put under a time-lapse microscope for imaging.

Microscopy

MDA-MB-231 distribution, viability and proliferation

For the cell distribution tests, the devices were imaged immediately after injection under a light microscope (Leica DM 4000, Wetzlar, Germany). Imaging of the attached MDA-MB-231 cells for measuring cell viability was performed using the same microscope (Leica DM 4000).

Fluorescent microscopy

Cell attachment

Following cell attachment on glass substrate after 6 hours in culture, the cells were stained and imaged under Leica DM 5500 fluorescent microscope (Wetzlar, Germany).

On-chip staining

Cells were incubated on-chip for 24 hours after which staining solution was loaded into the main channel of the device. After 1 hour incubation and washing steps, the devices were imaged using Axio Scop.A1 fluorescent microscope (Oberkochen, Germany).

Microscopy for MMP activity of single cancer cells

Leica DMi8 live cell imaging inverted microscope was adjusted to take transmitted and fluorescent images of all semi-droplets by defining the imaging starting point and end-point. The microscope software (LAS X, Leica Microsystems) divided the imaging area into imaging units and merged them after all images were obtained. Four exposure times of 1ms, 200ms, 500ms and 1s were used to make sure that at least one exposure time gives measurable data. Data from the optimum exposure time was then used.

Image and data analysis

Distribution, viability and proliferation analysis

Analysis of distribution, viability and proliferation was done by counting the number of cells in semi-droplets using ImageJ software (NIH, Bethesda, USA). The threshold was optimized

for each image to achieve separated and distinguishable cells with no background noise. The Particle Analysis tool was used to count the number of cells in each image.

MMP secretion measurement

To quantify the MMP activity of single MDA-MB-231 cancer cells, fluorescent signals out of each droplet were measured using ImageJ. On each image the region of interest (ROI) was selected which is the area occupied by each droplet that was defined using the Freehand Selection tool. Then in ROI manager under multi measure, mean grey value was measured for the selected area. Higher fluorescent intensity corresponds to higher enzyme secretion by the cells.

Theory

Device components and principle of operation

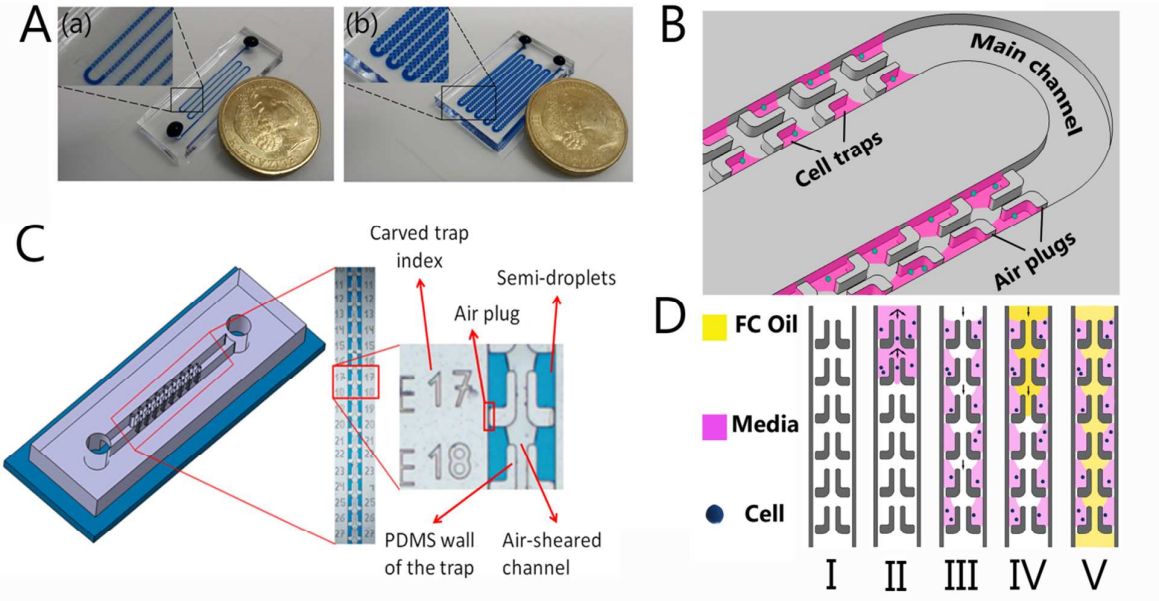

Figure 1: Schematic illustration of the high-throughput static droplet device configuration and operation. (A) Image of a chip with (a) 500×2.5nl droplet traps, (b) 600×14nl droplet traps with close-up image of the traps. (B) 3D schematic of the device showing the traps, air plug sites and the main channel. (C) Chip components including traps, semi-droplets, main channel, air plug and trap indices. (D) Device loading steps: (I) Empty device (II) Cell-containing medium is injected into the channel (III) air pressure shears the continuous liquid into separate semi-droplets (IV and V) Fluorocarbon oil is introduced at the inlet and flows to sheath the stationary semi-droplets.

A 3D schematic of the static droplet system along with the device filled with blue food colour is shown in Fig. 1A-C. It contains two parts; the main channel where the cell

suspension is flowing in and the trapping sites where cells are being captured. The trapping regions of the device are pairs of L-shaped equally-distanced obstacles. One of the main concerns in previous microfluidic chamber designs was cell-cell crosstalk between adjacent chambers due to the shared media. In the present device, neighbouring chambers are separated by a narrow gap of air plug which prevents drop-drop signalling and thus maintains each cell's chemical signature (Fig. 1B and Fig. S2). To be able to monitor cell behaviour over time, one needs to be able to precisely locate them. Although marking of the chip near each droplet's location is possible, it is not applicable since the sizes of the chip/chambers are too small. To address this issue, numbers were embedded near each trap (Fig 1C)[48]. This way, if for example a cell in trap E17 (Fig. 1C) is of interest, it can easily be found and tracked over time.

One of the issues with the current static droplet systems is that they need to produce droplets first and only then trap them in predefined positions. Syncing the number of droplets generated using active systems with the number of available traps is sometimes problematic and needs precise adjustments[37]. The device presented here is capable of simultaneously making droplets and allocating them to traps using only a single pipette injection. Furthermore, one can easily increase the number of traps using a serpentine structure. Using this method, we designed chips with 5 rows of 100 traps (total number of 500 traps) to accommodate as many single cells as possible.

The static droplet system operates in four steps, as shown in Fig 1D. A cell suspension is injected into the device using a standard lab pipette. The solution flows and fills both the channel and the traps. When a solution fills one pair of counter traps, the liquid/air interface reaches the narrow restriction which exhausts air while limiting further progress of the liquid due to opposing surface tension force which is imposed by Laplace pressure at the liquid-gas meniscus (Fig. 1D-II). When the flow of solution fills the second pair of counter traps, it

again pushes air out through the restriction site but simultaneously helps in shaping the air plug between the two adjacent trapping pairs. Following rapid cell sedimentation, the solution in the middle of the channel is blown with air using a standard lab pipette which shears the liquid and leads to the formation of liquid compartments (Fig 1D-III) (also see **Movie S1 and Movie S2**). The residue is collected with sterile filter papers at the outlet. Finally, fluorocarbon oil (Fluorinert FC40) is added to the channel and fills the middle part of the channel. Fluorocarbon oil plays two important roles: 1) it prevents extensive evaporation of the nanoliter-sized semi-droplets; 2) it enhances oxygen and CO_2 transfer to/out from the cells.

Design considerations

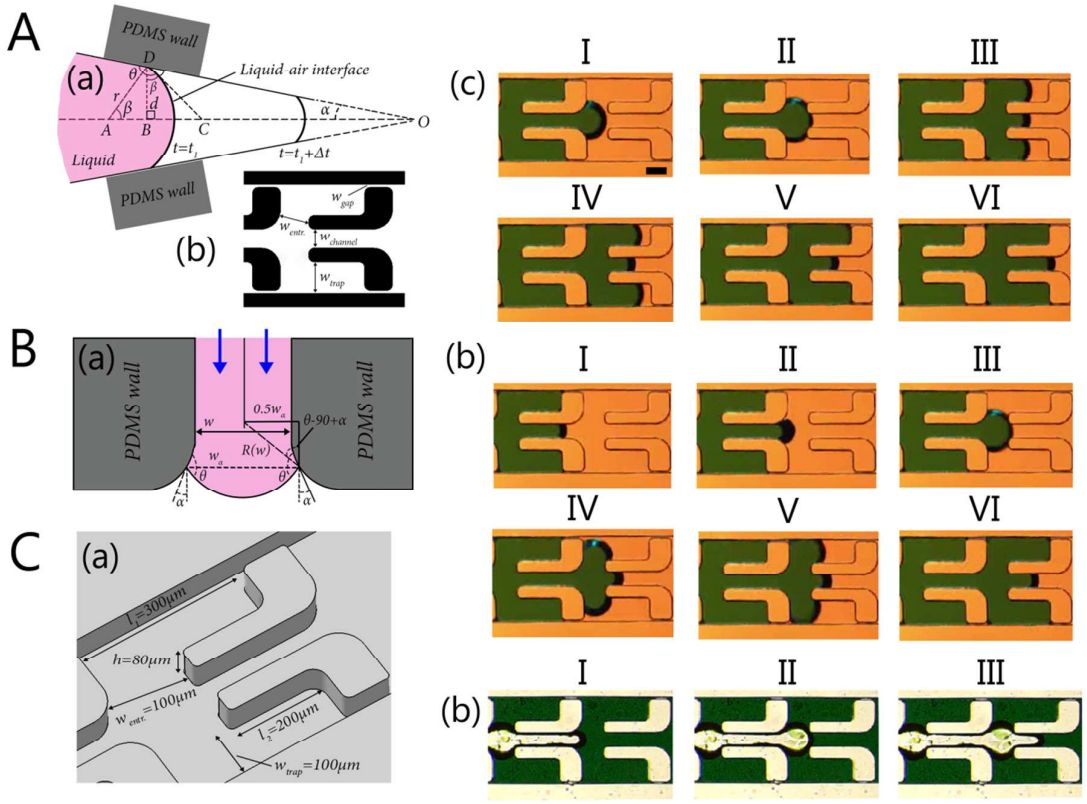

Figure 2: Device working mechanism (A) Tracking liquid-air interface in the channel: (a) Theoretical analysis of liquid-air interface movement in the channel and through the traps[50]; (b) Critical dimensions in the static droplet array device; (c) Time-lapse images of liquid-air interface movement while entering the traps: Liquid filling the previous traps first and then moving toward the next set of traps; Liquid-air interface just before entering the traps demonstrating the entrance length to the traps and the main channel. (B) (a)Theoretical analysis of liquid-air interface movement/blockage while passing through a geometrical change; (b) Liquid

stops at the narrow restriction but moves through the main channel; (C) Liquid shearing and droplet compartmentalization: (a) Critical dimensions in traps design; (b) Time-lapse image of liquid shearing in the main channel (Scale bar=100 μm).

In order to be able to design a functional static droplet device and predict the traps filling behavior, the physics of the flow in the channel as well as its relation with the geometry of the traps and channel dimensions should be carefully considered. Capillary pressure opposes the injection pressure, and therefore to make sure that the interface reaches certain locations at certain time points, pressure changes across the liquid-air interface needs to be calculated. Young-Laplace equation can therefore be used to find the interface's capillary pressure which reads,

$$\Delta P = -\gamma \overline{\nabla}.\hat{n} = 2\gamma H = \gamma(\frac{1}{R_1} + \frac{1}{R_2}) \quad (1)$$

Where ΔP is the pressure difference across the fluid interface called Laplace pressure, γ is the surface tension, $\hat{n}$ is the unit normal pointing out of the surface, H is the mean curvature, and R_1 and R_2 are the principle radii of curvature. Assuming that the interface is part of a cylinder with radius r, Eq.1 becomes

$$\Delta P = \frac{\gamma}{r} \quad (2)$$

To understand the effect of geometry on pressure, we will see how radius of curvature changes in the channel and through the traps. Fig. 2A demonstrates a schematic of fluid interface moving along PDMS channel walls[50]. In this figure, θ is the liquid-PDMS contact angle, α is the half of the opening angle of the channels (β=0 for a straight channel), $r=AD$ is the radius of curvature of the liquid-air interface, and d is the half-distance between the channel walls.

ΔCOD: $\theta = \alpha + (180^{\circ} - (90^{\circ} - \beta)) \rightarrow \beta = \theta - \alpha - 90^{\circ}$ (3)

ΔABD: $\sin(\beta) = d/r$ (4)

From (3) and (4) we can write,

$r = d/\sin(\beta) = d/\sin(\theta - \alpha - 90^{\circ})$ (5)

Combining (2) with (5),

$$P(x) = \gamma . \sin(\theta - \alpha - 90^{\circ})/d = \gamma . \cos(\theta - \alpha)/d \quad (6)$$

To better understand this formula, we review the fluid movement along the channel. Looking at Eq. 6 and Fig. 2Aa, when liquid-air interface moves from $t=t_1$ to $t= t_1+\Delta t$, the radius of curvature and consequently the value of d deceases leading to an increase in the capillary pressure value demanding higher injection pressure to fill the channel. Fig. 2Ab presents the geometry of a trap and the corresponding channel width in different locations. Fig. 2Ac-II demonstrates the moment when the liquid-air interface reaches a trap's entrance. Based on the above explanations, in order to ensure that the liquid first enters the trap and only after it fully filled the trap, it continues to fill the main channel (Fig. 2Ac-VI), it is essential to have $w_{entr.} > w_{channel}$; In this design these values are 100 μm and 70 μm respectively.

The fact that the filling pressure needs to be bigger than the capillary pressure to force the liquid to move in the channel necessitates consideration of any geometrical change that may increase the capillary pressure. Although increased capillary pressure can be balanced with the increased filling pressure, since the device is made to be in a temporary bond with the substrate, the range of the operating pressure is limited. Fig. 2Ba demonstrates such a condition[51]: For any given change in the channel geometry, there exists a burst pressure $\Delta P_{burst} = Max\left(\frac{2\gamma\cos(\theta+\alpha)}{w_\alpha}\right)$ which occurs at the interface's minimum radius of curvature $R_w = \frac{w_\alpha}{2\cos(\theta+\alpha)}$ and it is defined as the highest achievable capillary pressure at the liquid interface while moving through that geometry[51]. In the presented design, we have two positions with channel expansion. One when the liquid leaves the main channel and moves toward the traps. And the second one is at the narrow restriction site which functions as a stop valve (Fig. S3 and Movie S3). We made sure that the burst pressure in the main channel is low enough to let the liquid pass with a wide range of filling pressures and is high enough in the restriction to stop the liquid from further movement ($w_{channel}$ =70 μm vs w_{gap}=10 μm).

Fig S3-C also shows that the presence of narrow restriction is essential in the process of droplet trapping. If the restriction gets blocked (e.g. due to fabrication defect) the liquid cannot move into the traps (Movie S4). In addition, from Fig. 2Bb, it is clear that comparing liquid movement in the traps with the main channel, the interface moves faster in the trap which is wider ($w_{trap} > w_{channel}$).

In order to shear the liquid from the main channel and segment the liquid into semi-droplets in separate traps, the principle of surface energy minimization was taken into account. One such phenomenon takes place in splitting a sessile drop of radius a which is squeezed between parallel plates of distance δ. Assuming that γ_{SL} and γ_{LG} are the surface-liquid and liquid-gas interfacial tensions, the division of the drop requires an increase in surface energy of $\Delta E/E \approx (\sqrt{2}-1)/\sqrt{2}\left(1+\frac{\gamma_{SL}.a}{\gamma_{LG}.\delta}\right)$ [52]. If $a \gg \delta$ and $\gamma_{SL} > \gamma_{LG}$ this equation simplifies to $\Delta E/E \approx \frac{\gamma_{LG}.\delta}{\gamma_{SL}.a}$. This equation shows that to have droplet splitting, the liquid surface contact area should be maximized while liquid-air contact area should be minimized. Looking at Fig. 2Ca, this means that the trap's length and width should be maximized (the liquid-surface interfacial area) and its height and entrance width ($w_{entr.}$) should be minimized (the liquid-air interfacial area). However, decreasing the device height increases the capillary pressure limiting the range of operational filling pressure. In addition, increasing the trap length may impair device filling during the sample injection step[48]. Keeping these design considerations in mind, the device dimensions were chosen as shown in Fig. 2Ca. Fig. 2Cb shows liquid shearing from the main channel over time. Movie S5 and Movie S6 present the movement and location of all liquid-air and liquid-oil interfaces throughout the shearing and droplet sheathing steps respectively.

Results and discussion

Cell distribution, single cell trapping

In order to evaluate the trapping efficiency (The percentage of traps with only one cell/particle) and to have a rough estimation of the concentration which leads to the highest efficiency (saturation concentration), two sizes of 10.7µm and 19.2µm PMMA particles (Magsphere, Pasadena, CA, USA; CAT number: PM010UM and PM020UM) were used. Different concentrations of particles were prepared in MACS buffer solution (Miltenyi Biotec, Gladbach, Germany) and were injected into the device using a lab pipette (Fig. 1D). In order to be able to compare the effect of particle size, fixed values of concentrations were used (Fig. S4). The saturation concentration is 1×10^6/ml for 19.2 µm particles while for 10.7µm this does not happen even up to 2×10^6/ml. This is because bigger particles are able to deviate from the flow streamlines and fill the traps at low concentrations while at high concentrations (above saturation concentration) they have less space to move freely causing clogging at the trap's entrance.

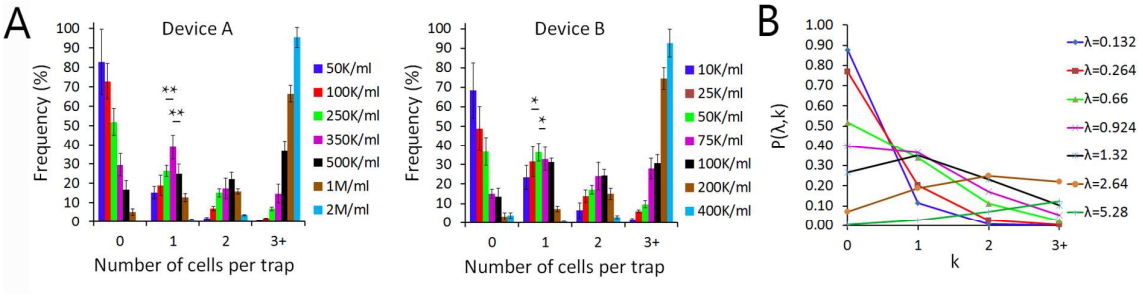

Figure 3: Device characterisation: Distribution of MDA-MB-231 breast cancer cells with a wide range of cell concentration in droplet arrays of different size (n=9, (*): $p<0.05$; (**): $p<0.01$); N=500 droplets. Poisson distribution function with λ values corresponding to MDA-MB-231 breast cancer cells with a wide range of cell concentration.

In order to assess cell trapping, two configuration of the device with different trapping size of 2.5nl (device A) and 14nl (device B) were used (Fig. 1A). Given the fact that the size of MDA-MB-231 cells are in the range of 15-20µm, cell trapping was performed with the same range of concentrations that were used in the particle trapping experiment to find the saturation concentration. It should be mentioned that as long as the injection flow rate is

within the device's operation range (i.e. 0.05-0.35µl/s) any change in trapping efficiency with the injection flow rate is negligible (See Fig. S5). Fig. 3A demonstrates cell occupancy in device A and device B. As can be seen in this figure, the saturation concentration for device A (2.5nl traps) and device B (14nl traps) are 3.5×10^5/ml and 5×10^4/ml respectively leading to highest trapping efficiency of 38.8% and 36.4% for device A and B respectively. Indeed, bigger traps can accommodate more cells and therefore to achieve single cell trapping one should use lower cell concentrations. For both devices, increasing the concentration leads to decreased number of empty traps but increased number of traps containing three and more cells.

Comparing the distribution of particles and cells in droplets (i.e. Fig. S4 and Fig. 3A), it is found that the results have differences especially at higher concentrations. This was predictable since cells and particles are different in their size distribution (particles are more uniform in size), deformability (cells are more deformable), density (PMMA particles density is around 1.2 gr/ml while cells density is around 1gr/ml), and shape (particles are more homogeneous in shape)[53-55]. Deformability for example was shown to cause lateral migration of cells enabling them to cross the flow streamlines in the channel[56].

Fig. 3B demonstrates the Poisson distribution $p(\lambda, k) = \frac{\lambda^k e^{-\lambda}}{k!}$ which is used to estimate the number of cells per droplet in typical non-deterministic single cell trapping methods [57]. In this equation k is the number of particles in a droplet and λ is the average number of cells per droplet volume and can be defined as the ratio between the volume fraction of cells in the pre-encapsulation solution $\emptyset_s$ and that of a droplet containing one cell $\emptyset_d$ (Calculation for λ, $\emptyset_s$ and $\emptyset_d$ values are presented in SI- **method S1** and **Table S1**). Here $p(\lambda, k)$ is calculated based on the λ values corresponding to different cell concentrations in device A. In theory, the maximum efficiency for trapping single cells takes place when $\lambda = 1$ at 37%. With regard to the Poisson distribution (Fig. 3B) which is plotted for the same concentrations as of our

experiments, it is indicated that the maximum single cell trapping efficiency is 36.67% for 3.5×10^5/ml (λ=0.924). In the same concentration, the device shows single cell trapping efficiency of 38.8% (percentage error=5.8%).

In order to evaluate the device endurance under pipette/pumping pressure; five clean devices were brought into contact to glass/tissue culture substrate and then loaded with a syringe filled with water raised at different heights (see **method S2** and **Fig. S6**). As can be seen in Fig.S6, when in contact with a glass substrate, the device can maintain leakage-free operation at higher pressures compared to a plastic substrate.

Cell culture, viability, proliferation and on-chip staining

Cells were cultured in a device which was temporarily sealed against a TC/glass substrate. To overcome the issue of low-volume droplet evaporation which is shared among droplet-based systems, PDMS devices were soaked in water overnight and at the time of culture a humidity chamber was created (Fig S1). Unlike other droplet methods here each droplet is supported by TC/glass substrate providing cell attachment and preventing anoikis or cell apoptosis[58, 59]. Some of the challenges with long-term cell culturing in single cell devices are droplet evaporation, and nutrient depletion. Therefore, cell viability is important to ensure that culture condition has not compromised cells functionality or inadvertently caused rapid cell death. To ensure that there is enough nutrients for single cells to grow in each trap, cell culture surface, volume and their ratio were calculated in each design. For device A (2.5nl traps), these values are 3.3×10^{-4} cm^2, 2.5 nl, and 12.5 respectively. For device B (14nl traps) these values are 1.79×10^{-3} cm^2, 14 nl and 12.5 respectively. For both designs, the surface to volume ratio is within the recommended range suggested by Halldorsson et al.[62].

To assess the device capability in maintaining cells function, we measured viability and proliferation over 48 hours culture period. MDA-MB-231 cells were prepared at each device's saturation concentration and viability was measured after 12 hours, 18 hours, 24

hours and 48 hours culture using Trypan Blue staining (see Materials and methods) which makes live/dead cells easily distinguishable as shown in Fig. 4A. To quantify viability, five chips were imaged at each time point and viability was calculated as the number of live cells to the total number of cells. It can be seen from Fig. 4B that cell viability remains> 85% in most of the experiments. The minimum viability was 81% for device A (2.5nl traps) at 48 hours and was 81% compared to 87% for device B (14nl traps) ($p<0.05$, $n=5$). We therefore conclude that the trap size plays an important role in maintaining cells viability in long-term culture of single cells in droplets. The functionality of the cultured cells in terms of their proliferation rate was investigated. We observed high proliferation of single cells giving 1.338 and 1.579 times increase in the number of cells in device A and B respectively ($p<0.05$, $n=5$). Comparing proliferation of cells in two devices, it can be seen that cells proliferate better in bigger droplets.

One capability of the device presented here is access to cells following culture owing to the reversible bond between the PDMS device and the culture substrate. This capability can facilitate complicated and time-consuming single cell assays[60, 61]. A pair of tweezers can be used to gently peel the device followed by addition of culture media (Method S3). As shown in Fig. S7, peeling the device from the TC substrate provides access to individual cells by maintaining the trace of the channel walls as well as the trap indices due to binding of nutrients, protein molecules and dye in phenol red following device peel off and evaporation of droplets. Unlike TC substrate, glass substrate does not preserve the trace of the channel but still provides access to single cells.

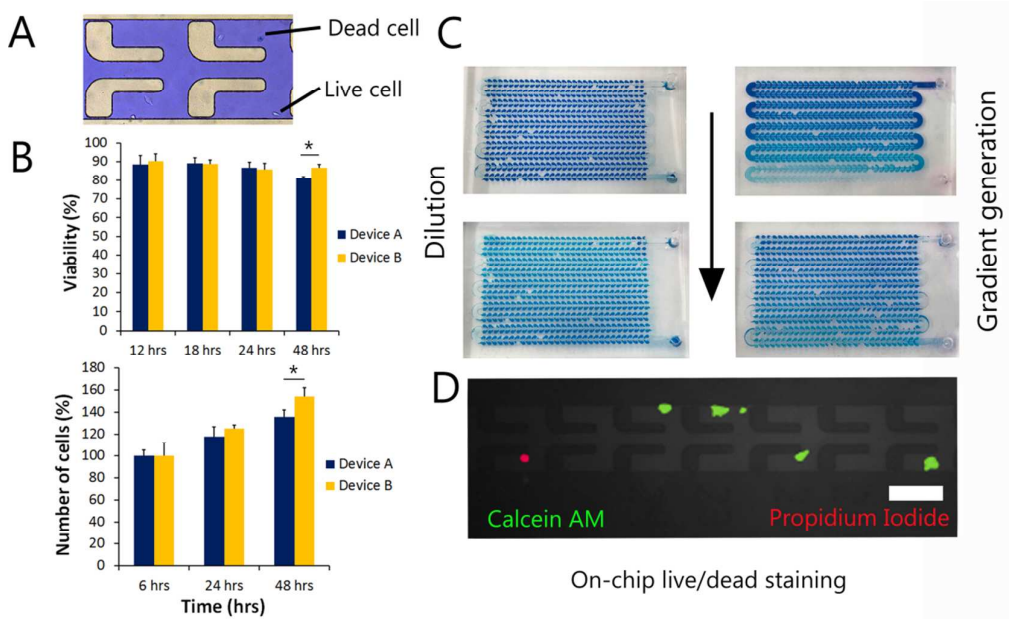

Figure 4: Cell and solute treatment in the device. (A) On-chip cell viability assay in each droplet; cells were cultured in the droplets for 12 hrs, 18 hrs, 24 hrs, and 48 hrs after which Trypan blue was injected into the device; Dead cells uptake Trypan blue and can be distinguished from the live cell. (B) On-chip measurement of cell viability and proliferation over time in device A and B. ($p<0.05$, $n=5$); N=500 droplets (C) Left: On-chip solute dilution: the device was first filled with blue food dye followed by injection of a water plug. The droplet dilutes the solute in each trap; the size of the droplet defines the dilution factor. Right: Solute gradient formed in droplet array device: The device was first filled with pure water followed by shearing liquid from the main channel and injection of a plug of blue food dye. Shearing the food dye will leave the device with droplets containing gradient of food dye. (D) On-chip staining of cells by adding live/dead staining solution to the droplets content (calcein AM and propidium iodide) after 24 hours culturing period (Scale bar=300µm).

Given the ability of the device to trap single cells, we studied the possibility of changing the content of droplets providing a pathway to on-chip access to the cells and droplets chemical composition. This capability was shown before using a variety of methods[38, 45, 63, 64] and can help in miniaturizing high-throughput screening assays[45, 65]. The method introduced here can be used both for droplet dilution or gradient generation and can be done in four simple steps. Dilution of droplets content starts with injecting the sample into the device and shearing the residual liquid from the main channel (Fig. 4C-left). Next, the diluting liquid is introduced into the main channel and is sheared. In order to make gradients of solute in static droplets (Fig. 4C-right), first low concentration solute is injected into the device followed by shearing the excess liquid from the main channel. Next, a plug of high concentration solute (blue food dye) is injected into the device and gradient was achieved by shearing the main channel for the second time. For both dilution and gradient generation, the concentration of the

concentrate solute, and the size of the plug determine the dilution factor/the gradient steepness in the droplet array. For example increasing the size of the water plug will increase the dilution factor (Fig. S8A). Using multistep sample injection, the device enables generating gradients of two solutes, and changing the gradient steepness (Fig S8B and –S8C). In order to show a potential application of sample dilution in the device, cells were cultured in the device over 24 hours. Following oil removal from the main channel, live/dead double staining solution with concentration of 4 μM was injected into the device. After 1 hour incubation, the staining solution was removed and cells were washed multiple times by injecting PBS. Fig. 4D demonstrates fluorescent image of the stained cells superposing phase contrast, green and red channels revealing cells live/dead status. Live cells uptake calcein AM and will become green while dead cells uptake propidium iodide and are shown in red. Since this dilution can be done several times, sequential reactions on single cell level can be operated with a simple microfluidic device.

Single cancer cell proteolytic assay

Proteolytic degradation of the extracellular matrix (ECM) is known to be a determinant factor in cancer invasion and metastasis. In this process, cancer cells release degrading enzymes that cleave the ECM protein[66]. This highlights the importance of studying proteolytic activity of cells for development of novel protease targeting drugs. An established method for studying such an activity is based on observing the fluorescent intensity out of the reaction between the released enzyme and a protease-sensitive substrate known as fluorescence resonance energy transfer (FRET) substrate[67]. Conventional proteolytic assays measure average activity of the cells masking the fact that cancer invasion due to proteolytic activity is driven by the heterogeneity between cancer cells[68]. In addition, knowing the proteolytic activity of different subclones may lead to more effective treatment strategies[8].

The static droplet system developed in this study enables tracking the proteolytic activity of individual cancer cells over time. Cells were mixed with FRET substrate in 1:1 ratio and trapped in semi-droplets in the device. The frequency of fluorescent traps that have no cells, one cell, two cells or more follows the Poisson distribution (average values are 33.6%, 38.5%, 16.7% and 11.2% respectively). Using time-lapse microscopy, dynamic MMP activity of single cells was monitored. Fig. 5A demonstrates clear difference between fluorescent intensity of droplets across the device. Fig. 5A-b shows two semi-droplets containing one cell but with different fluorescent signal indicating different level of MMP activity among single cancer cells. Measurement of relative fluorescent intensity (Fig. 5A-c) shows that semi-droplets containing more cells produce stronger signals, i.e., droplets containing two cells are brighter than those containing one cell or no cells ($p<0.001$). To demonstrate the capability of the device in measuring cell dynamics behavior, fluorescent intensity of each semi-droplet containing no cells, one cell or two cells were measured over a period of 14 hours and plotted in Fig. 5B. The MMP activity increases over time. The experimental data is also represented in a heat map showing heterogeneity between MMP activity of single cells and semi-droplets containing different number of cells over time. Fig. S9 presents the relative fluorescent intensity in the droplets with the same number of cells in individual heat maps as well as the number of cells in each trap and their corresponding fluorescent intensity.

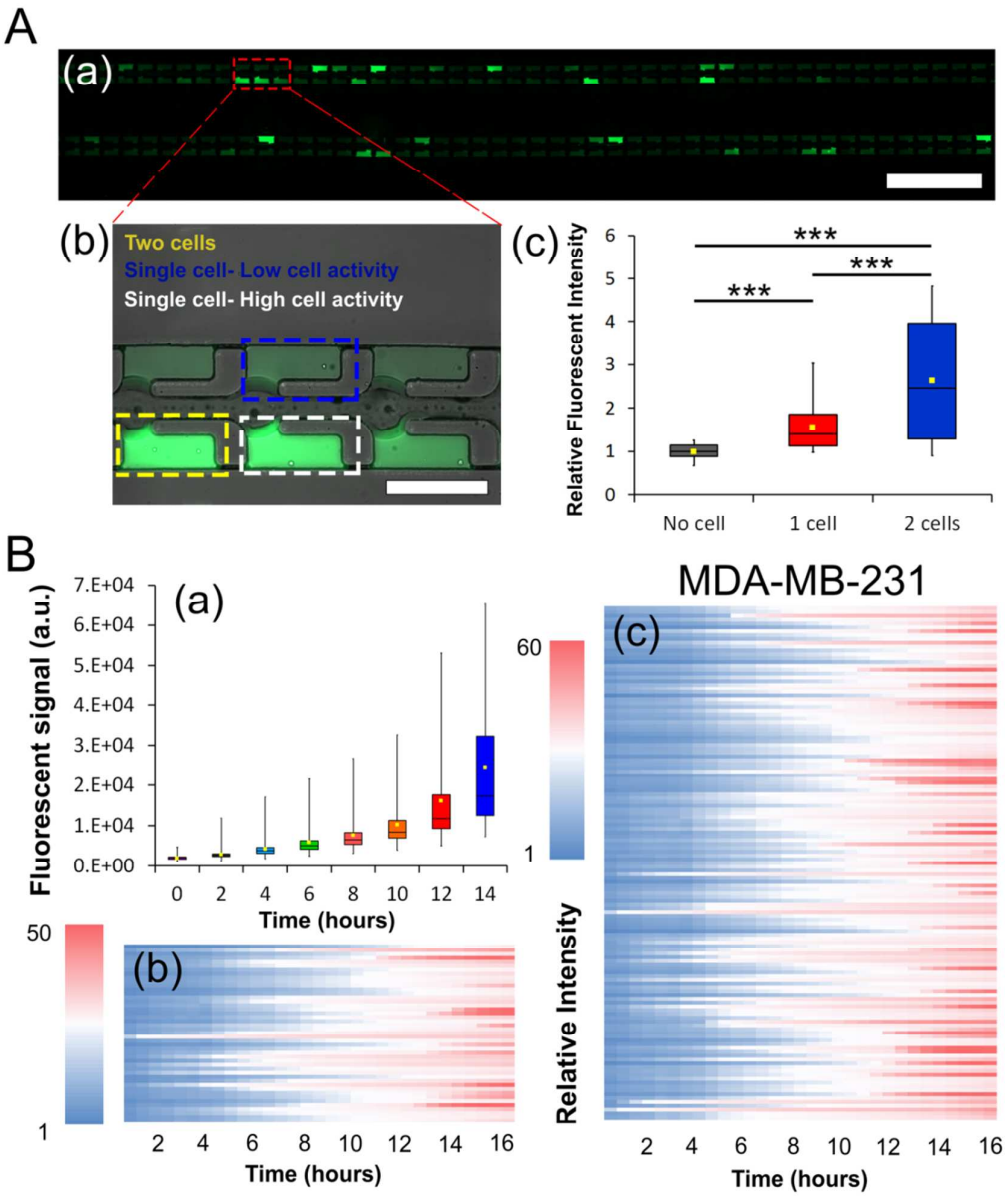

Figure 5: MMP assay at the single cell level of MDA-MB-231 cancer cell line. (A) Relative fluorescent intensity in semi-droplets (a) an array showing the fluorescent signal out of different semi-droplets, Scale bar: 1.5mm (b) zoomed view demonstrating droplets with no cell, high activity and low activity single cell with their corresponding fluorescent signal, Scale bar: 300 µm, (c) A box plot demonstrating the relative fluorescent intensity of each chamber with no cell, one cell or two cells at a certain time point; as expected droplets containing one cell have higher fluorescent signal compared to empty droplets and droplets with two cells are brighter than those containing one cell (N=102 for cases with no cell, N=114 for cases with one cell and N=53 for cases with two cells), P≤0.001, n=3. (B) Single cell MMP activity over time (a) fluorescent intensity of droplets over time showing increase in MMP activity in droplets during the course of 14 hours in culture. (b), (c) Cellular heterogeneity and dynamic response; heat map presenting the relative fluorescent intensity in droplets containing one cell in (b) and different number of cells (0, 1, or 2 per droplet) in (c). Red color represents high MMP activity and blue color shows low MMP activity.

Concluding remarks

In summary, a novel leakage-free static droplet array system with a built-in valving mechanism was introduced that is able to rapidly and reliably capture single cells in chemically isolated indexed traps and in a high-throughput manner. The presented device enables long-term culture and dynamic monitoring of cells for periods of hours up to days. This was successfully assessed by capturing the heterogeneity among single cancer cells MMP activity over time. Droplet generation happens in three simple steps of filling, shearing, and sheathing. We explained critical design considerations of the static droplet array including selection of the width of the channel in different channel locations and presented a guideline for analyzing the behavior of liquid-air interface in the device. We also demonstrated two important device capabilities: post-culture access to cells through simple device peel off and on-chip manipulation of droplets content.

The overall setup and injection procedure of this unique design takes less than 10 minutes, does not require any microfluidic expertise and is operated with standard laboratory pipette which makes it a suitable choice for biologist and other end users. To the best of our knowledge and compared to its previous counterparts, the presented device is the simplest device for single cell trapping and analysis to date. We therefore believe that this method may open up new opportunities and lead to fast-tracking single cell discoveries.

Author contributions

A.H.-B, and M.E.W. conceived the idea of the study. A.H.-B, A.L., A.H. performed the experiments. A.H.-B, A.H. collected and analyzed the data. A.H.-B wrote the draft of the paper. M.A., D.G.-O, C. O. and M.E.W. commented on the manuscript. All authors discussed the results and reviewed the manuscript.

Conflicts of interest

There are no conflicts to declare.

Acknowledgements

This work was performed (in part) at the NSW and South Australian node of the Australian National Fabrication Facility under the National Collaborative Research Infrastructure Strategy to provide nano- and microfabrication facilities for Australia's researchers. We would like to thank Dr. Nadia Court and Joanna Szymanska from ANFFNSW for their professional technical support regarding the SOI wafer fabrication. Cells were kindly provided by Garvan Institute of Medical Research/the Kinghorn Cancer Centre and the catalogue number is cited in the text. A.H.-B would like to thank Dr. William Hughes from Garvan Institute of Medical Research for his guidance and help in live-cell imaging. We also thank Dr. Jonathan Shemesh for his help in fabrication of the device and providing comments by reading the paper. We would like to acknowledge Dr. Tracie Barber for providing feedback and enriching the manuscript. M.E.W. would like to acknowledge the support of the Australian Research Council through Discovery Project Grants (DP170103704 and DP180103003) and the National Health and Medical Research Council through the Career Development Fellowship (APP1143377).

References

1. A. Saadatpour, S. Lai, G. Guo and G.-C. Yuan, *Trends in genetics : TIG*, 2015, **31**, 576-586.
2. N. E. Navin, *Genome Research*, 2015, **25**, 1499-1507.
3. L. Wen and F. Tang, *Genome Biology*, 2016, **17**, 71.
4. S. A. Kobel, O. Burri, A. Griffa, M. Girotra, A. Seitz and M. P. Lutolf, *Lab on a Chip*, 2012, **12**, 2843-2849.
5. P. K. Chattopadhyay, T. M. Gierahn, M. Roederer and J. C. Love, *Nature Immunology*, 2014, **15**, 128.
6. C. Ma, R. Fan, H. Ahmad, Q. Shi, B. Comin-Anduix, T. Chodon, R. C. Koya, C.-C. Liu, G. A. Kwong, C. G. Radu, A. Ribas and J. R. Heath, *Nature Medicine*, 2011, **17**, 738.
7. A. Zeisel, A. B. Muñoz-Manchado, S. Codeluppi, P. Lönnerberg, G. La Manno, A. Juréus, S. Marques, H. Munguba, L. He, C. Betsholtz, C. Rolny, G. Castelo-Branco, J. Hjerling-Leffler and S. Linnarsson, *Science*, 2015, **347**, 1138.
8. S. J. Altschuler and L. F. Wu, *Cell*, **141**, 559-563.
9. A. Hassanzadeh-Barforoushi, J. Shemesh, N. Farbehi, M. Asadnia, G. H. Yeoh, R. P. Harvey, R. E. Nordon and M. E. Warkiani, *Scientific Reports*, 2016, **6**, 35618.
10. A. Marusyk and K. Polyak, *Biochimica et Biophysica Acta (BBA) - Reviews on Cancer*, 2010, **1805**, 105-117.
11. H. Dueck, J. Eberwine and J. Kim, *BioEssays*, 2016, **38**, 172-180.
12. C. Gawad, W. Koh and S. R. Quake, *Nature Reviews Genetics*, 2016, **17**, 175.

13. I. Kanter and T. Kalisky, *Frontiers in Oncology*, 2015, **5**.
14. A. J. Hughes, D. P. Spelke, Z. Xu, C.-C. Kang, D. V. Schaffer and A. E. Herr, *Nature Methods*, 2014, **11**, 749.
15. K. J. Son, A. Rahimian, D.-S. Shin, C. Siltanen, T. Patel and A. Revzin, *Analyst*, 2016, **141**, 679-688.
16. J. Yuan and P. A. Sims, *Scientific Reports*, 2016, **6**, 33883.
17. D. J. Collins, B. Morahan, J. Garcia-Bustos, C. Doerig, M. Plebanski and A. Neild, *Nature Communications*, 2015, **6**, 8686.
18. H. Chen, J. Sun, E. Wolvetang and J. Cooper-White, *Lab on a Chip*, 2015, **15**, 1072-1083.
19. K. J. Park, K. G. Lee, S. Seok, B. G. Choi, M.-K. Lee, T. J. Park, J. Y. Park, D. H. Kim and S. J. Lee, *Lab on a Chip*, 2014, **14**, 1873-1879.
20. L. Armbrecht and P. S. Dittrich, *Analytical Chemistry*, 2017, **89**, 2-21.
21. Z. B. Bjornson, G. P. Nolan and W. J. Fantl, *Current Opinion in Immunology*, 2013, **25**, 484-494.
22. R. K. Cheung and P. J. Utz, *Nature Reviews Rheumatology*, 2011, **7**, 502.
23. D. Muzzey and A. van Oudenaarden, *Annual Review of Cell and Developmental Biology*, 2009, **25**, 301-327.
24. J. W. Young, J. C. W. Locke, A. Altinok, N. Rosenfeld, T. Bacarian, P. S. Swain, E. Mjolsness and M. B. Elowitz, *Nature Protocols*, 2011, **7**, 80.
25. L. Mazutis, J. Gilbert, W. L. Ung, D. A. Weitz, A. D. Griffiths and J. A. Heyman, *Nature protocols*, 2013, **8**, 870-891.
26. H. N. Joensson and H. Andersson Svahn, *Angewandte Chemie International Edition*, 2012, **51**, 12176-12192.
27. C. Holtze, S. Weisse and M. Vranceanu, *Micromachines*, 2017, **8**, 193.
28. C.-G. Yang, Z.-R. Xu and J.-H. Wang, *TrAC Trends in Analytical Chemistry*, 2010, **29**, 141-157.
29. M. G. Simon and A. P. Lee, in *Microdroplet Technology: Principles and Emerging Applications in Biology and Chemistry*, eds. P. Day, A. Manz and Y. Zhang, Springer New York, New York, NY, 2012, DOI: 10.1007/978-1-4614-3265-4_2, pp. 23-50.
30. M. C. Draper, C. R. Crick, V. Orlickaite, V. A. Turek, I. P. Parkin and J. B. Edel, *Analytical Chemistry*, 2013, **85**, 5405-5410.
31. H. R. Holmes and K. F. Böhringer, *Microsystems &Amp; Nanoengineering*, 2015, **1**, 15022.
32. S. K. Küster, S. R. Fagerer, P. E. Verboket, K. Eyer, K. Jefimovs, R. Zenobi and P. S. Dittrich, *Analytical Chemistry*, 2013, **85**, 1285-1289.
33. J. L. Garcia-Cordero and Z. H. Fan, *Lab on a Chip*, 2017, **17**, 2150-2166.
34. Y. Sun, X. Zhou and Y. Yu, *Lab on a Chip*, 2014, **14**, 3603-3610.
35. C. H. J. Schmitz, A. C. Rowat, S. Koster and D. A. Weitz, *Lab on a Chip*, 2009, **9**, 44-49.
36. A. Huebner, D. Bratton, G. Whyte, M. Yang, A. J. deMello, C. Abell and F. Hollfelder, *Lab on a Chip*, 2009, **9**, 692-698.
37. S. Sarkar, N. Cohen, P. Sabhachandani and T. Konry, *Lab on a Chip*, 2015, **15**, 4441-4450.
38. E. Fradet, C. McDougall, P. Abbyad, R. Dangla, D. McGloin and C. N. Baroud, *Lab on a Chip*, 2011, **11**, 4228-4234.
39. M. Junkin, Alicia J. Kaestli, Z. Cheng, C. Jordi, C. Albayrak, A. Hoffmann and S. Tay, *Cell Reports*, 2016, **15**, 411-422.
40. D. E. Cohen, T. Schneider, M. Wang and D. T. Chiu, *Analytical Chemistry*, 2010, **82**, 5707-5717.
41. H.-H. Jeong, B. Lee, S. H. Jin, S.-G. Jeong and C.-S. Lee, *Lab on a Chip*, 2016, **16**, 1698-1707.
42. M. Sun, S. S. Bithi and S. A. Vanapalli, *Lab on a Chip*, 2011, **11**, 3949-3952.
43. A. Dewan, J. Kim, R. H. McLean, S. A. Vanapalli and M. N. Karim, *Biotechnology and Bioengineering*, 2012, **109**, 2987-2996.
44. K. Leung, H. Zahn, T. Leaver, K. M. Konwar, N. W. Hanson, A. P. Pagé, C.-C. Lo, P. S. Chain, S. J. Hallam and C. L. Hansen, *Proceedings of the National Academy of Sciences*, 2012, **109**, 7665-7670.
45. H.-H. Jeong, S. H. Jin, B. J. Lee, T. Kim and C.-S. Lee, *Lab on a Chip*, 2015, **15**, 889-899.

46. P. Mehlen and A. Puisieux, *Nature Reviews Cancer*, 2006, **6**, 449.
47. S. S. Bithi and S. A. Vanapalli, *Scientific Reports*, 2017, **7**, 41707.
48. J. Shemesh, T. Ben Arye, J. Avesar, J. H. Kang, A. Fine, M. Super, A. Meller, D. E. Ingber and S. Levenberg, *Proceedings of the National Academy of Sciences*, 2014, **111**, 11293-11298.
49. J. Avesar, D. Rosenfeld, M. Truman-Rosentsvit, T. Ben-Arye, Y. Geffen, M. Bercovici and S. Levenberg, *Proceedings of the National Academy of Sciences*, 2017, **114**, E5787-E5795.
50. J. Berthier, in *Micro-Drops and Digital Microfluidics (Second Edition)*, William Andrew Publishing, 2013, DOI: https://doi.org/10.1016/B978-1-4557-2550-2.00002-X, pp. 7-73.
51. B. Hagmeyer, F. Zechnall and M. Stelzle, *Biomicrofluidics*, 2014, **8**, 056501.
52. J. Berthier, in *Micro-Drops and Digital Microfluidics (Second Edition)*, William Andrew Publishing, 2013, DOI: https://doi.org/10.1016/B978-1-4557-2550-2.00005-5, pp. 225-301.
53. J. P. Beech, S. H. Holm, K. Adolfsson and J. O. Tegenfeldt, *Lab on a Chip*, 2012, **12**, 1048-1051.
54. A. Karimi, S. Yazdi and A. M. Ardekani, *Biomicrofluidics*, 2013, **7**, 021501.
55. Z. Zhang, E. Henry, G. Gompper and D. A. Fedosov, *The Journal of Chemical Physics*, 2015, **143**, 243145.
56. S. K. Doddi and P. Bagchi, *International Journal of Multiphase Flow*, 2008, **34**, 966-986.
57. D. J. Collins, A. Neild, A. deMello, A.-Q. Liu and Y. Ai, *Lab on a Chip*, 2015, **15**, 3439-3459.
58. S. M. Frisch and R. A. Screaton, *Current Opinion in Cell Biology*, 2001, **13**, 555-562.
59. Y.-C. Chen, Y.-H. Cheng, H. S. Kim, P. N. Ingram, J. E. Nor and E. Yoon, *Lab on a Chip*, 2014, **14**, 2941-2947.
60. Evan Z. Macosko, A. Basu, R. Satija, J. Nemesh, K. Shekhar, M. Goldman, I. Tirosh, Allison R. Bialas, N. Kamitaki, Emily M. Martersteck, John J. Trombetta, David A. Weitz, Joshua R. Sanes, Alex K. Shalek, A. Regev and Steven A. McCarroll, *Cell*, 2015, **161**, 1202-1214.
61. A. K. Shalek, R. Satija, J. Shuga, J. J. Trombetta, D. Gennert, D. Lu, P. Chen, R. S. Gertner, J. T. Gaublomme, N. Yosef, S. Schwartz, B. Fowler, S. Weaver, J. Wang, X. Wang, R. Ding, R. Raychowdhury, N. Friedman, N. Hacohen, H. Park, A. P. May and A. Regev, *Nature*, 2014, **510**, 363.
62. S. Halldorsson, E. Lucumi, R. Gómez-Sjöberg and R. M. T. Fleming, *Biosensors and Bioelectronics*, 2015, **63**, 218-231.
63. S.-W. Hu, B.-Y. Xu, W.-k. Ye, X.-H. Xia, H.-Y. Chen and J.-J. Xu, *ACS Applied Materials & Interfaces*, 2015, **7**, 935-940.
64. S. S. Bithi, W. S. Wang, M. Sun, J. Blawzdziewicz and S. A. Vanapalli, *Biomicrofluidics*, 2014, **8**, 034118.
65. M. Davenport, K. E. Mach, L. M. D. Shortliffe, N. Banaei, T.-H. Wang and J. C. Liao, *Nature Reviews Urology*, 2017, **14**, 296.
66. A. Das, M. Monteiro, A. Barai, S. Kumar and S. Sen, *Scientific Reports*, 2017, **7**, 14219.
67. G. B. Fields, in *Matrix Metalloproteinase Protocols*, ed. I. M. Clark, Humana Press, Totowa, NJ, 2010, DOI: 10.1007/978-1-60327-299-5_24, pp. 393-433.
68. A. Chapman, L. Fernandez del Ama, J. Ferguson, J. Kamarashev, C. Wellbrock and A. Hurlstone, *Cell Reports*, 2014, **8**, 688-695.

Rapid and reliable capture and analysis of single cells in chemically isolated static droplet array for fast-tracking single cell discoveries.

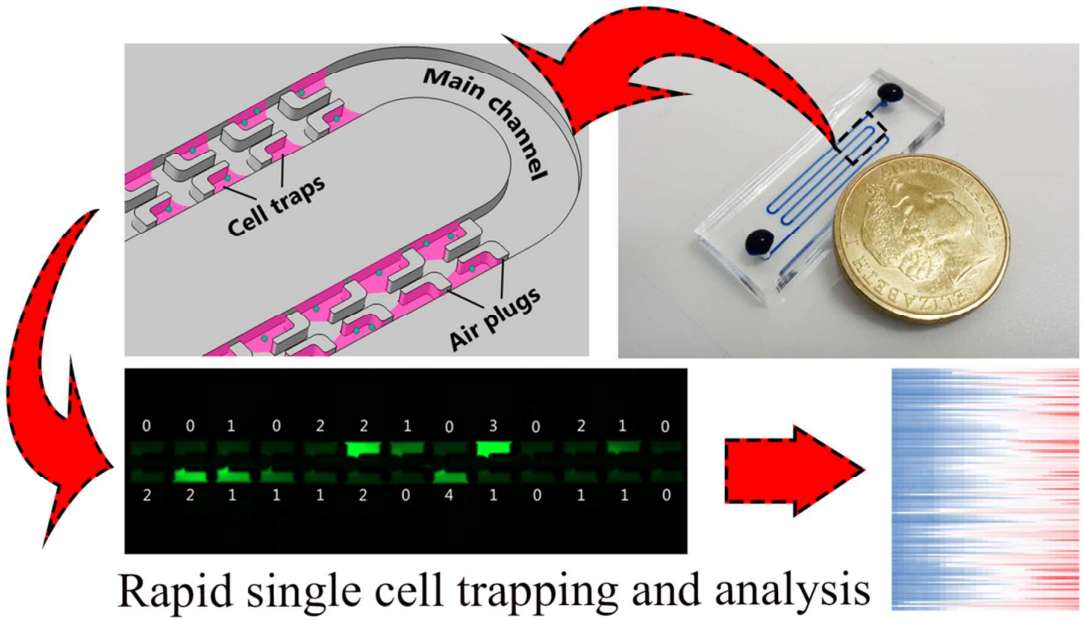

Rapid single cell trapping and analysis